

## Linearly Polarized Remote-Edge Luminescence in GaSe Nanoslabs

Yanhao Tang,<sup>1</sup> Wei Xie,<sup>1</sup> Krishna C. Mandal,<sup>2</sup> John A. McGuire,<sup>1</sup> and Chih Wei Lai<sup>1,\*</sup>

<sup>1</sup>*Department of Physics and Astronomy, Michigan State University, East Lansing, Michigan 48824, USA*

<sup>2</sup>*Department of Electrical Engineering, University of South Carolina, Columbia, South Carolina 29208, USA*

(Received 21 February 2015; revised manuscript received 7 May 2015; published 24 September 2015)

We report highly linearly polarized remote luminescence that emerges at the cleaved edges of nanoscale gallium selenide slabs tens of micrometers away from the optical excitation spot. The remote-edge luminescence (REL) measured in the reflection geometry has a degree of linear polarization above 0.90, with polarization orientation pointing toward the photoexcitation spot. The REL is dominated by an index-guided optical mode that is linearly polarized along the crystalline  $c$  axis. This luminescence is from out-of-plane dipoles that are converted from in-plane dipoles through a spin-flip process at the excitation spot.

DOI: 10.1103/PhysRevApplied.4.034008

### I. INTRODUCTION

Two-dimensional layered materials present a new platform for integration of optoelectronic devices and nanoscale lasers [1–4]. In this paper, we exploit the anisotropic optical properties [5–10] and unique optical selection rules [11–13] in layered gallium selenide (GaSe) to generate highly linearly polarized luminescence at the remote cleaved edges of GaSe slabs of about 200 layers or more [Fig. 1(a)]. The in-plane dipoles ( $d_{\perp}$ ) generated at the photoexcited spot are converted to out-of-plane dipoles ( $d_{\parallel}$ ) through a spin-flip process. Subsequent luminescence from  $d_{\parallel}$  propagates with a wave vector orthogonal to the incident optical excitation beam through an index-guided optical mode that is linearly polarized along the crystalline  $c$  axis. Remote luminescence emerges at the cleaved edges in the reflection geometry as a result of backscattering. This remote-edge luminescence (REL) has a degree of linear polarization above 0.90, with polarization orientation pointing toward the photoexcitation spot independent of the photoexcitation polarization. In contrast, the luminescence at the photoexcited focal spot (FL) is unpolarized under a linearly polarized optical excitation.

In most bulk semiconductors, the optical orientation and alignment of electron-hole ( $e$ - $h$ ) pairs and consequent polarized luminescence are limited [14]. In quasi-2D systems, such as semiconductor quantum wells, photoluminescence is typically unpolarized or circularly polarized, depending on the photoexcitation energy and polarization as well as the band structure. Highly linearly polarized luminescence or lasing has been observed in quasi-1D colloidal nanowires [15–17] with strong dielectric confinement, as well as in quasi-0D quantum dots with a sizable anisotropy induced by strain or electron-hole exchange interactions [18–21]. Recently, in 2D atomically

thin transition-metal dichalcogenides (TMDs), polarized luminescence has been shown to result from intra- and interlayer excitations [22] or valley coherence [23,24]. In 2D TMDs, though, the luminescence yield becomes significant only at the monolayer level when a crossover from indirect to direct gap occurs.

GaSe is a layered semiconductor characterized by covalently bound gallium and selenium atoms within a single layer and weak van der Waals-type interlayer interactions [25]. The layers are stacked along the crystallographic  $c$  axis and form several polytypes with different stacking orders. The noncentrosymmetric  $\epsilon$ -GaSe is the most widely studied of the group-III monochalcogenides because of its high optical second-order nonlinearity [25–27]. The layered structure of  $\epsilon$ -GaSe results in highly anisotropic optical properties, as demonstrated by the distinct absorbance for light with  $\vec{E} \perp c$  and  $\vec{E} \parallel c$  [5–10]. Polarized spontaneous and stimulated emissions also occur near the quasidirect gap ( $E_g \sim 2$  eV) under optical excitation and detection at oblique angles [28–36]. Nanoscale slabs of similar polar (pyroelectric) group-III monochalcogenide semiconductors have high optical nonlinearities and allow direct optical access for control of light-matter interactions and polarization properties, as well as index guiding of light.

### II. RESULTS

In this study, we investigate the spectral, *polarization*, and *dynamic* characteristics of the luminescence emanating at cleaved edges of GaSe slabs with a thickness  $d_L$  of 160 nm or more. The GaSe nanoslabs are mechanically exfoliated from a bulk  $\epsilon$ -GaSe crystal [37] and deposited onto a Si substrate with a 90-nm SiO<sub>2</sub> layer. These GaSe dielectric slabs on SiO<sub>2</sub>/Si form the simplest optical waveguides (see Materials and Methods) [38]. The thinnest GaSe that can sustain one guided TE mode ( $\vec{E} \perp c$ ) and TM mode ( $\vec{E} \parallel c$ ) for luminescence near the band edge

\*cwlai@msu.edu

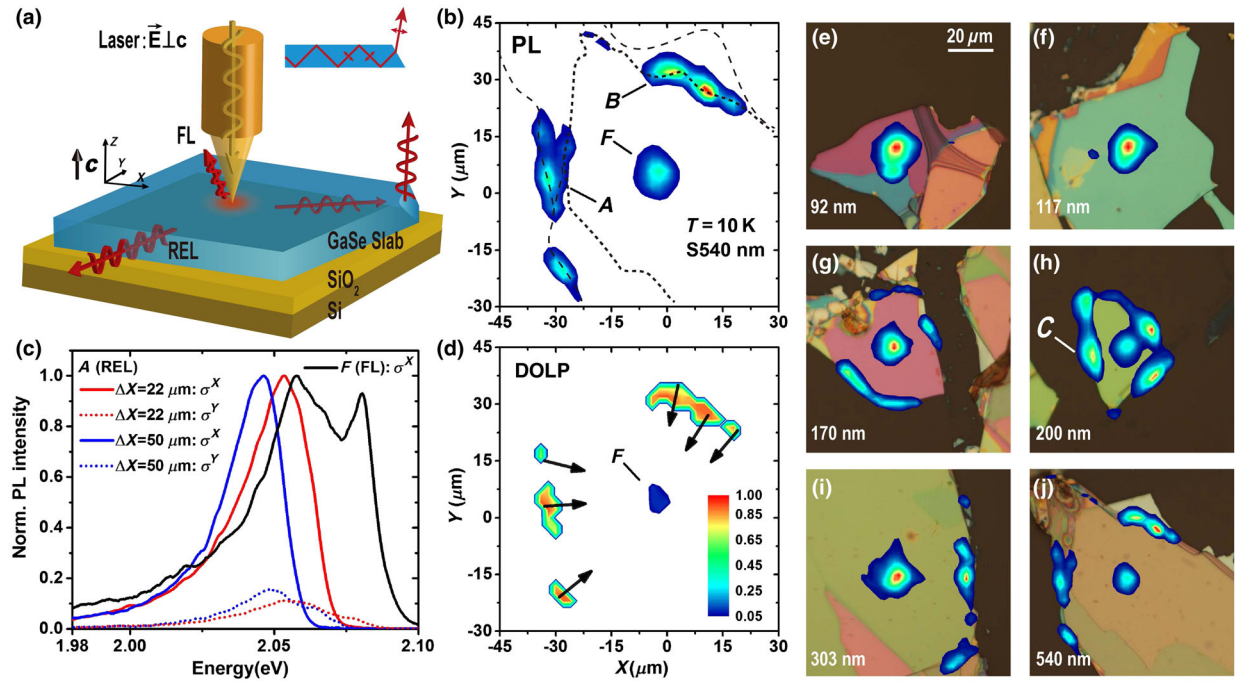


FIG. 1. (a) Schematic of the optical setup. (b) Photoluminescence (PL) image of a 540-nm-thick GaSe slab at  $T = 10$  K. The sample is optically pumped at the focal location  $F$  under a pump flux  $P = 0.1P_0$ , where  $P_0 = 2.6 \times 10^{14}$   $\text{cm}^{-2}$  per pulse. At  $P_0$ , the photoexcited carrier density is about  $3.4 \times 10^{17}$   $\text{cm}^{-3}$  ( $2.7 \times 10^{10}$   $\text{cm}^{-2}$  per layer). The dashed lines represent the cleaved edges of the sample. REL emerges at the cleaved edges tens of micrometers away from the photoexcited spot. (c) Polarized spectra of the FL (black curve) from focal point  $F$  and the REL (red and blue curves) from location  $A$  with varying distances ( $\Delta X$ ) from the photoexcited spot for  $P = 0.15 P_0$  at  $T = 10$  K. The spectra are normalized with respect to the  $X$ -polarized ( $\sigma^X$ ) component. Both  $\sigma^X$  [transverse-magnetic (TM) mode, solid lines] and  $\sigma^Y$  [transverse-electric (TE) mode, dashed lines] spectral components redshift with respect to the FL with increasing  $\Delta X$  as a result of anisotropic reabsorption. The anisotropic reabsorption also results in a decreasing spectrally integrated degree of linear polarization (DOLP) with increasing  $\Delta X$ . The two peaks in the FL spectrum are attributed to free excitons (approximately 2.08 eV) and exciton-carrier scattering (approximately 2.06 eV), respectively. The FL is dominated by free excitons for  $P \gtrsim 0.6P_0$  (not shown). (d) Spatially resolved DOLP for  $P = 0.1P_0$ . The false color and arrows represent the DOLP and polarization orientation, respectively. The measured maximal DOLP is about 0.93. Note that the REL at location  $A$  [Fig. 1(c)] is  $X$  polarized, whereas the REL at location  $B$  is nearly  $Y$  polarized. The REL has a polarization oriented toward the photoexcited spot. (e)–(j) Overlay of optical and luminescence images of samples with thickness  $d_L = 92, 117, 170, 200$  (S200nm), 303, and 540 (S540nm). Luminescence images are measured at  $T = 10$  K. The false colors in the luminescence images represent the relative intensities. The colors in the optical images are due to optical interference. The REL is visible only for  $d_L \gtrsim 160$  nm. The central elliptical luminescence spot is the focal photoexcited region. The REL is most prevalent in the 200-nm-thick sample in which single-guided TE and TM modes are present.

(wavelength  $\lambda \approx 600$  nm) is about 160 nm thick. The normally incident 2-ps optical excitation pulses create in-plane dipoles ( $d_{\perp}$ ) that are rapidly converted to out-of-plane dipoles ( $d_{\parallel}$ ) through spin flip of electrons or holes [Fig. 1(a)] [11–13]. The index-guided radiation from  $d_{\parallel}$  at the photoexcited spot propagates to the cleaved edges of the GaSe slabs. Under pulsed photoexcitation, the guided TM mode of  $d_{\parallel}$  luminescence dominates over the TE mode of  $d_{\perp}$  luminescence because the radiative recombination rate of  $d_{\parallel}$  is about 30 times higher than that of  $d_{\perp}$ . As a result, highly linearly polarized TM mode luminescence emerges in the reflection geometry at cleaved edges when back-scattering is allowed. We refer to such polarized remote luminescence at cleaved edges as REL. The REL typically has a degree of linear polarization  $\text{DOLP} > 0.90$ . Note that enhanced PL has also been observed at photoexcited edges

of  $\text{WS}_2$  platelets [39]. In the experiments presented in this paper, the in-plane ( $d_{\perp}$ ) and out-of-plane ( $d_{\parallel}$ ) dipoles are within the same layer, and the REL occurs tens of micrometers away from the photoexcited spot.

In Fig. 1, we study the spectral and polarization characteristics of the REL from a 540-nm-thick GaSe slab under excitation energy  $E_p = 2.138$  eV at  $T = 10$  K. Intense luminescence emerges at the cleaved edges of the GaSe slab even when the optical excitation spot is tens of micrometers away [Fig. 1(b)]. Spectrally, the REL shows an apparent redshift compared with the luminescence at the FL. Additionally, the REL is highly linearly polarized ( $\text{DOLP} \rightarrow 0.93$ ), whereas the FL is unpolarized under linearly polarized photoexcitation [Fig. 1(d)]. Considering the REL as an index-guided mode of luminescence originating from the photoexcited spot, one can

attribute the spectral redshift to anisotropic reabsorption [33] when luminescence propagates in plane for a distance of tens of micrometers [Fig. 1(c)]. However, for a 540-nm-thick GaSe dielectric slab on SiO<sub>2</sub>, about four guided TE modes and TM modes are allowed. In the presence of both TE and TM modes, the REL is expected to be unpolarized when the orientations of the photoexcited dipoles at the focal spot are random and isotropic. On the contrary, the measured luminescence polarization image [Fig. 1(d)] indicates that the polarization orientations of the REL point toward the photoexcited spot. Moreover, depending on the location and sample thickness, the intensity (emission flux) of the REL can exceed that of the FL [Figs. 1(f)–1(j)]. Such a polarization orientation pattern and intensity distribution suggest that the REL originates from out-of-plane dipoles ( $d_{\parallel}$ ), with the electric-field vector parallel to the crystalline  $c$  axis ( $\vec{E} \parallel c$ ).

To understand the unique polarization of the REL, we need to consider the selection rules and anisotropic optical constants in GaSe. We first examine the optical selection rules in GaSe and illustrate the spin-flip-induced conversion between the in-plane and out-of-plane dipoles (Fig. 2). The Se  $4p_z$  states lie 1.2 and 1.6 eV above the Se  $4p_{x,y}$  states as a result of the crystal field and spin-orbit interaction. Near the  $\Gamma$  point, direct optical transitions between the  $p_z$ -like uppermost valence band and  $s$ -like lowermost conduction band are dipole allowed for light with the electric field parallel to the  $c$  axis ( $\vec{E} \parallel c$ ). For light

with  $\vec{E} \perp c$ , the transitions become weakly allowed due to spin-orbit interaction [7]. The spin-dependent optical selection rules can be best understood in the two-particle (exciton) representation [Fig. 2(a)] [11,12]. Optical excitation with  $\vec{E} \perp c$  creates excitons with  $\Gamma_6$  symmetry ( $d_{\perp}$  dipoles), which is analogous to a triplet state ( $\uparrow\uparrow$  and  $\downarrow\downarrow$ ). On the other hand, optical excitation with  $\vec{E} \parallel c$  results in excitons with  $\Gamma_4$  symmetry ( $d_{\parallel}$  dipoles), which is analogous to a singlet state ( $\uparrow\downarrow - \downarrow\uparrow$ ). Therefore, a spin flip of either electron or hole of the exciton ( $e$ - $h$  pair) results in the conversion between  $d_{\perp}$  and  $d_{\parallel}$  [Fig. 2(b)].

Experimentally, the absorption coefficient near the band edge for  $\vec{E} \perp c$  is about  $3 \times 10^3 \text{ cm}^{-1}$ , which is a factor of 1/30 of that for light with  $\vec{E} \parallel c$ . Assuming that the spontaneous radiative recombination rate is proportional to the absorption coefficient, we approximate the relative radiative recombination rates of the in-plane and out-plane dipoles to be  $W_{\parallel}^r/W_{\perp}^r \approx 30$ . As a result, under picosecond pulse excitation, luminescence is dominated by the radiative recombination of  $d_{\parallel}$  when the conversion between  $d_{\perp}$  and  $d_{\parallel}$  is fast compared with the recombination rates. The linear polarization of the REL is approximately  $(W_{\parallel}^r - W_{\perp}^r)/(W_{\parallel}^r + W_{\perp}^r) \approx 0.94$ , which is consistent with the measured DOLP.

In Fig. 3, we study the spectral and dynamic characteristics of the REL at room temperature. The REL remains highly linearly polarized, with a polarization orientation pointing to the photoexcited spot. The FL and REL are nearly synchronized temporally without an identifiable time delay in the REL. Therefore, the REL cannot originate from carriers that are photoexcited at the focal spot and transported to the cleaved edges. We attribute the REL to the backscattered light from an index-guided optical TM mode with  $\vec{E} \parallel c$ . The  $d_{\parallel}$  converted from the photoexcited  $d_{\perp}$  radiates into this TM mode, which propagates in plane from the photoexcited spot to the cleaved edges at the speed of light in the GaSe slab. The sub-10-ps rise time of the REL in Fig. 3 indicates that energy relaxation and conversion of photoexcited  $d_{\perp}$  and  $d_{\parallel}$  are less than 10 ps at room temperature [11–13].

The spin-flip-induced conversion between the in-plane and out-of-plane dipoles is evident in the time-dependent PL measurements at cryogenic temperature ( $T = 10 \text{ K}$ ), where the spin-flip rate is significantly reduced (Fig. 4). The FL arises within 10 ps after the pulse excitation, whereas the REL reaches its maximum about 50 ps afterward. The nearly instantaneous rise of the FL is the result of a sub-5-ps energy-momentum relaxation of photoexcited carriers, whereas the considerable delay of approximately (30–50)-ps rise time of the REL is due to the approximately 30-ps spin-flip time constant at  $T = 10 \text{ K}$ .

A model for the time- and spin-dependent dynamics of the lowest-energy excitons has been described elsewhere [40].

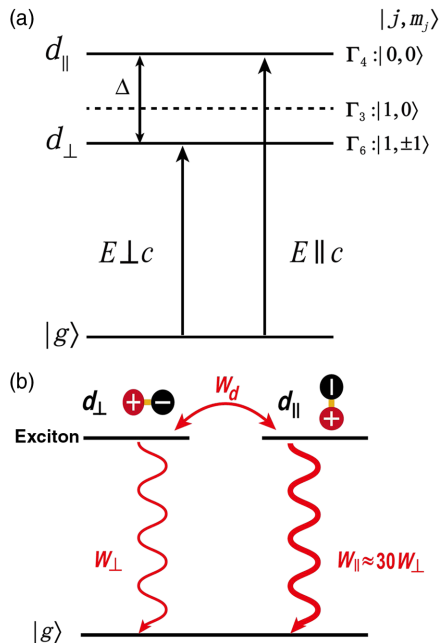


FIG. 2. (a) Schematic exciton levels in  $\epsilon$ -GaSe at the  $\Gamma$  point and the representations to which the states at the  $\Gamma$  point belong when including spin-orbit interaction. The energy splitting  $\Delta$  between the  $\Gamma_4$  ( $d_{\parallel}$ ) and  $\Gamma_6$  ( $d_{\perp}$ ) exciton states is approximately 2 meV [11,12]. (b) Schematic of the rate equation model.

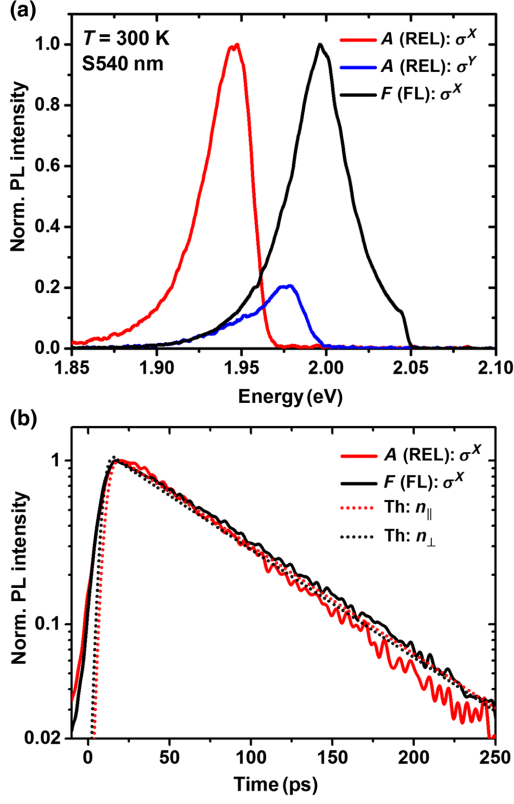


FIG. 3. (a) Polarized spectra of the FL (black curve) and the REL from location A (red and blue curves) in a 540-nm-thick GaSe slab at room temperature. The pump energy  $E_p = 2.087$  eV and the pump flux  $P = 1.0 P_0$ . At room temperature, the FL is largely due to free excitons, and the backscattered REL intensity is considerably weaker than the FL (about a factor of 4 here). The DOLP is above 0.93 for  $E < 1.95$  eV, where the anisotropic reabsorption for  $\sigma^X$  (TM mode) and  $\sigma^Y$  (TE mode) is negligible. (b) Time-dependent FL and REL. The FL (solid black curve) and the REL (solid red curve) show similar rise and decay times. The dotted black (red) curve is the calculated  $n_{\perp}$  ( $n_{\parallel}$ ), which corresponds to the time-dependent luminescence from  $d_{\perp}$  ( $d_{\parallel}$ ) dipoles. The theoretical curves are calculated with a rate equation model and convolved with an 8-ps (FWHM) instrument response. The fitting parameters are as follows:  $W_{\perp}^r = 1/1000$  (ps $^{-1}$ ),  $W_{\parallel}^r = 30 W_{\perp}^r$ ,  $W_d = 1/3$  (ps $^{-1}$ ).

In the case that either  $k_B T$  or the inhomogeneous linewidth ( $\Gamma_h$ ) of the exciton transitions is much larger than  $\Delta$ , the polarized time-dependent luminescence is reproduced by a simplified model in which the spin-flip rates  $W_{\parallel,\perp}$  describing scattering from  $d_{\perp}$  to  $d_{\parallel}$ , and  $W_{\perp,\parallel}$  are set equal to one another. Considering a spin-flip process and anisotropic radiative recombination rates for the in-plane and out-of-plane dipoles, we describe the time-dependent FL and REL with the following set of coupled differential equations:

$$\begin{aligned} \dot{n}_{\perp}(t) &= -W_{\perp}^r n_{\perp}(t) - W_d [n_{\perp}(t) - n_{\parallel}(t)] + G(t)P, \\ \dot{n}_{\parallel}(t) &= -W_{\parallel}^r n_{\parallel}(t) + W_d [n_{\perp}(t) - n_{\parallel}(t)]. \end{aligned}$$

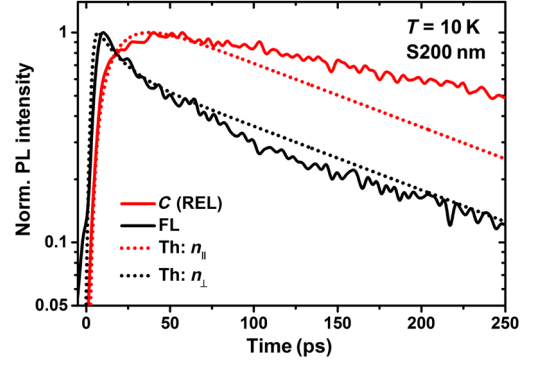


FIG. 4. Time-dependent FL (solid black line) and REL (solid red line) in a 200-nm-thick sample (S200nm). The REL is measured at location C, as indicated in Fig. 1(h). The dotted black (red) line is the calculated time-dependent  $n_{\perp}$  ( $n_{\parallel}$ ) convolved with a 4-ps (FWHM) instrument response function. The fitting parameters are as follows:  $W_{\perp}^r = 1/2000$  (ps $^{-1}$ ),  $W_{\parallel}^r = 30 W_{\perp}^r$ ,  $W_d = 1/30$  (ps $^{-1}$ ). The slower decay of the REL relative to the FL is likely due to reabsorption, which results in the dominance of the REL by the low-energy portion of the exciton luminescence.

The optical generation rate is approximated by a 2-ps Gaussian pulse  $G(t)P$ , where  $P$  is the pump flux.  $n_{\perp}$  and  $n_{\parallel}$  are the populations of the in-plane ( $d_{\perp}$ ) and out-of-plane ( $d_{\parallel}$ ) dipoles, whereas  $W_{\perp}^r$  and  $W_{\parallel}^r$  are the corresponding radiative recombination rates.  $W_d$  is the spin-flip rate that leads to the conversion between  $d_{\perp}$  and  $d_{\parallel}$ . In this simple model, we neglect the energy relaxation of nonresonantly excited carriers and nonradiative recombination loss. The time-dependent REL agrees with the calculated temporal evolution of  $n_{\parallel}$  and indicates a rise time of approximately 30 ps that is consistent with the previously measured spin-flip time constant  $\tau_s \approx 1/W_d$  [13]. Similarly, the time-dependent FL is associated with the temporal evolution of  $n_{\perp}$ . When  $\Gamma_h, k_B T \lesssim \Delta$ , one must account for the differences in spin-flip rates  $W_{\parallel,\perp}$  and  $W_{\perp,\parallel}$ . For the experimental conditions considered here, though,  $\Gamma_h \approx \Delta$  [41] yielding results similar to those obtained from the simplified equations above.

In summary, we observe highly linearly polarized remote-edge luminescence in GaSe platelets with a thickness of 160 nm or more. The REL is due to the guided TM mode of luminescence from the out-of-plane dipoles that are converted from the in-plane dipoles photoexcited by normally incident picosecond pulses at a remote spot.

### III. DISCUSSION

Anisotropic absorption and TE-polarized emission of excitons have also been observed for light propagating in the quantum-well plane in GaAs-based structures. In the absence of mixing of the heavy-hole and light-hole bands, the emission from heavy-hole excitons propagating in

the quantum-well plane (in plane) is expected to be TE polarized [42]. In practice, a sample with quantum wells imbedded in a proper waveguide structure is required for the observation of remote polarized edge emission [43–46]. For example, the edge emission from GaAs-AlGaAs multiple quantum wells in a waveguide structure was measured to be TE polarized with a degree of linear polarization about 0.8 under excitation near or in resonance with heavy-hole excitons [43,44]. The reduced linear polarization as compared to the ideal unity linear polarization [42,47] was attributed to the presence of valence subbands with mixed  $M_j = \pm 3/2$  (heavy-hole) and  $M_j = \pm 1/2$  (light-hole) characters [43].

Lasing [48,49] or an enhanced spontaneous-emission rate [50–53] has been observed for atomically thin TMDs integrated with a microcavity (Fabry-Pérot [50,51], photonic crystals [48,52,53], or microdisk [49]). One can anticipate linearly polarized stimulated emission or lasing in microdisks with a thickness of approximately 200–300 nm and a lateral size of several micrometers when optical cavity effects are enhanced and nonradiative annihilation processes are suppressed [54]. Here, the GaSe layers will provide both gain and optical confinement and, in principle, should allow for in-plane integration with other photonic components [55–57].

## IV. MATERIALS AND METHODS

### A. Sample preparation

GaSe nanoslabs are mechanically exfoliated from a Bridgman grown GaSe crystal [37] and deposited onto a 90-nm SiO<sub>2</sub>/Si substrate. The samples studied here are mainly the  $\epsilon$  modifications. An  $\epsilon$ -GaSe crystal has ABA stacking of the individual layers and belongs to space group  $D_{3h}^1/P\bar{6}m2$  (no. 187) and point group  $D_{3h}$ . An individual layer consists of four planes of Se-Ga-Ga-Se, with the Ga—Ga bond normal to the layer plane arranged on a hexagonal lattice and the Se anions located in the eclipsed conformation when viewed along the  $c$  axis. The band-edge luminescence and absorption in  $\epsilon$ -GaSe are around 630 nm (2.0 eV) and 595 nm (2.1 eV) at room temperature and  $T = 10$  K, respectively. Samples are attached to a copper cold finger in an optical liquid-helium-flow cryostat and kept in a vacuum for all optical measurements.

### B. Optical setups

A 2-ps pulse laser beam is focused through an objective (N.A. = 0.28) to an area of about 80  $\mu\text{m}^2$ . As a result, the electric-field vector of the pump laser is orthogonal to the crystalline  $c$  axis ( $\vec{E} \perp c$ ). The photoexcitation density is from approximately  $2 \times 10^{16} \text{ cm}^{-3}$  to  $3.4 \times 10^{17} \text{ cm}^{-3}$  ( $2.7 \times 10^{-10} \text{ cm}^{-2}$  per layer) considering the absorption coefficient at 2.1 eV (approximately  $10^3 \text{ cm}^{-1}$  for  $\vec{E} \perp c$ ) and Fresnel loss from reflection. The photoexcited

density is below the Mott transition density in GaSe [35,36], which is about  $4 \times 10^{17} \text{ cm}^{-3}$ . The PL is collected through the same objective in a reflection geometry. The time-integrated PL spectra are measured with an imaging spectrometer (focal length, 750 mm; grating, 300 grooves/mm) equipped with a liquid-nitrogen-cooled CCD camera. The time-resolved PL measurements are obtained with a streak camera system with approximately (4–10)-ps (FWHM) temporal resolution depending on the exposure time. The polarization properties of the pump laser and PL are controlled and analyzed by a combination of polarizers and liquid-crystal devices without mechanical moving parts.

### C. Polarization

Linearly polarized light with horizontal (vertical) polarization is defined as  $\sigma^X$  ( $\sigma^Y$ ). The circularly polarized pump or luminescence with angular momentum  $+\hbar$  ( $-\hbar$ ) along the pump laser wave vector  $\hat{k} \parallel \hat{z}$  is defined as  $\sigma^+$  ( $\sigma^-$ ). The polarization state is characterized by the Stokes vector  $\{S_0, S_1, S_2, S_3\}$ .  $S_0$  is the flux and is determined as  $S_0 = I^X + I^Y$ . The Stokes vector can be normalized by its flux  $S_0$  to the Stokes three-vector  $s = \{s_1, s_2, s_3\}$ .  $s_1 = (I^X - I^Y)/S_0$ ,  $s_2 = (I^{45^\circ} - I^{135^\circ})/S_0$ , and  $s_3 = (I^+ - I^-)/S_0$ .  $I^+$ ,  $I^-$ ,  $I^X$ ,  $I^Y$ ,  $I^{45^\circ}$ , and  $I^{135^\circ}$  are measured intensities of the circularly or linearly polarized components. The degree of linear polarization is represented by  $\text{DOLP} \equiv \sqrt{s_1^2 + s_2^2}$ , and the polarization orientation angle is determined by  $\tan^{-1}(s_2/s_1)$ . The accuracy of the measurements of the DOLP are within 1–2%.

### D. Guided TE and TM modes [38]

We define a parameter  $V = (n_1^2 - n_2^2)^{1/2} k d_L$ , which includes the difference in the squares of the refractive indices of the core (i.e.,  $n_1$  of the GaSe slab) and the substrate (i.e.,  $n_2$  of the SiO<sub>2</sub> layer), the vacuum wavelength ( $\lambda_0$ ) and wave number ( $2\pi/\lambda_0$ ), and the thickness of the core slab ( $d_L$ ). The total number of TE or TM modes is then determined by the following equation:

$$N = \frac{1}{\pi} \left[ V - \arctan \left( \eta \sqrt{\frac{n_2^2 - n_3^2}{n_1^2 - n_2^2}} \right) \right]_{\text{int}},$$

where  $n_3$  is the refractive index of the capping layer (here vacuum), and the symbol  $[\ ]_{\text{int}}$  indicates that  $N$  is the integer part of the number in brackets. The parameter  $\eta$  is defined as

$$\eta = \begin{cases} 1, & \text{for TE modes,} \\ n_1^2/n_3^2, & \text{for TM modes.} \end{cases}$$

The number of TE and TM modes is usually the same for most  $d_L$ . However, the number of TE modes can exceed

that of the number of TM modes by one for specific ranges of  $d_L$  because  $n_1/n_3 > 1$ . For example, two TE modes and one TM mode exist for  $243 \text{ nm} \lesssim d_L \lesssim 276 \text{ nm}$ . Using  $n_1 = 3.00$  (GaSe),  $n_2 = 1.46$  (SiO<sub>2</sub>),  $n_3 = 1.00$  (vacuum), and  $\lambda_0 = 600 \text{ nm}$  (band-edge exciton luminescence at  $T \sim 10 \text{ K}$ ), we determine the thickness required to sustain only one guided TM mode and one TE mode to be about 162 to 242 nm.

### ACKNOWLEDGMENTS

This work is supported by National Science Foundation Grant No. DMR-09055944 as well as startup funding and the Cowen endowment at Michigan State University. This research has used the W. M. Keck Microfabrication Facility. We thank Norman Birge, Brage Golding, and Bhanu Mahanti for discussions.

- 
- [1] A. K. Geim and I. V. Grigorieva, Van der Waals heterostructures, *Nature (London)* **499**, 419 (2013).
- [2] G. Eda and S. A. Maier, Two-dimensional crystals: Managing light for optoelectronics, *ACS Nano* **7**, 5660 (2013).
- [3] P. Miró, M. Audiffred, and T. Heine, An atlas of two-dimensional materials, *Chem. Soc. Rev.* **43**, 6537 (2014).
- [4] G. Fiori, F. Bonaccorso, G. Iannaccone, T. Palacios, D. Neumaier, A. Seabaugh, S. K. Banerjee, and L. Colombo, Electronics based on two-dimensional materials, *Nat. Nanotechnol.* **9**, 768 (2014).
- [5] M. Schlüter, The electronic structure of GaSe, *Nuovo Cimento Soc. Ital. Fis.* **13B**, 313 (1973).
- [6] A. Bourdon and F. Khelladi, Selection rule in the fundamental direct absorption of GaSe, *Solid State Commun.* **9**, 1715 (1971).
- [7] A. Mercier, E. Mooser, and J. P. Voitchovsky, Near edge optical absorption and luminescence of GaSe, GaS and of mixed crystals, *J. Lumin.* **7**, 241 (1973).
- [8] R. Le Toullec, N. Piccioli, M. Mejatty, and M. Balkanski, Optical constants of  $\epsilon$ -GaSe, *Nuovo Cimento Soc. Ital. Fis.* **38B**, 159 (1977).
- [9] N. Piccioli, R. Le Toullec, M. Mejatty, and M. Balkanski, Refractive index of GaSe between  $0.45 \mu\text{m}$  and  $330 \mu\text{m}$ , *Appl. Opt.* **16**, 1236 (1977).
- [10] R. Le Toullec, N. Piccioli, and J. C. Chervin, Optical properties of the band-edge exciton in GaSe crystals at 10 K, *Phys. Rev. B* **22**, 6162 (1980).
- [11] E. M. Gamarts, E. L. Ivchenko, M. I. Karaman, V. P. Mushinskii, G. E. Pikus, B. S. Razbirin, and A. N. Starukhin, Optical orientation and alignment of free excitons in GaSe during resonance excitation. Experiment, *Sov. Phys. JETP* **46**, 590 (1977).
- [12] E. L. Ivchenko, G. E. Pikus, B. S. Razbirin, and A. I. Starukhin, Optical orientation and alignment of free excitons in GaSe under resonant excitation. Theory, *Sov. Phys. JETP* **45**, 1172 (1977).
- [13] Y. Tang, W. Xie, K. C. Mandal, J. A. McGuire, and C. W. Lai, Optical and spin polarization dynamics in GaSe nanoslabs, *Phys. Rev. B* **91**, 195429 (2015).
- [14] F. Meier and B. P. Zakharchenya, *Optical Orientation* (Elsevier, New York, 1984).
- [15] J. Hu, L.-S. Li, W. Yang, L. Manna, L.-W. Wang, and A. P. Alivisatos, Linearly polarized emission from colloidal semiconductor quantum rods, *Science* **292**, 2060 (2001).
- [16] J. Wang, M. S. Gudiksen, X. Duan, Y. Cui, and C. M. Lieber, Highly polarized photoluminescence and photo-detection from single indium phosphide nanowires, *Science* **293**, 1455 (2001).
- [17] J. C. Johnson, H. Yan, P. Yang, and R. J. Saykally, Optical cavity effects in ZnO nanowire lasers and waveguides, *J. Phys. Chem. B* **107**, 8816 (2003).
- [18] T. Takagahara, Effects of dielectric confinement and electron-hole exchange interaction on excitonic states in semiconductor quantum dots, *Phys. Rev. B* **47**, 4569 (1993).
- [19] D. Gammon, E. S. Snow, B. V. Shanabrook, D. S. Katzer, and D. Park, Homogeneous linewidths in the optical spectrum of a single gallium arsenide quantum dot, *Science* **273**, 87 (1996).
- [20] R. I. Dzhioev, B. P. Zakharchenya, E. L. Ivchenko, V. L. Korenev, Y. G. Kusraev, N. N. Ledentsov, V. M. Ustinov, A. E. Zhukov, and A. F. Tsatsul'nikov, Optical orientation and alignment of excitons in quantum dots, *Phys. Solid State* **40**, 790 (1998).
- [21] M. Paillard, X. Marie, P. Renucci, T. Amand, A. Jbeli, and J. M. Gerard, Spin Relaxation Quenching in Semiconductor Quantum Dots, *Phys. Rev. Lett.* **86**, 1634 (2001).
- [22] J. A. Schuller, S. Karaveli, T. Schiros, K. He, S. Yang, I. Kymissis, J. Shan, and R. Zia, Orientation of luminescent excitons in layered nanomaterials, *Nat. Nanotechnol.* **8**, 271 (2013).
- [23] A. M. Jones, H. Yu, N. J. Ghimire, S. Wu, G. Aivazian, J. S. Ross, B. Zhao, J. Yan, D. G. Mandrus, D. Xiao, W. Yao, and X. Xu, Optical generation of excitonic valley coherence in monolayer WSe<sub>2</sub>, *Nat. Nanotechnol.* **8**, 634 (2013).
- [24] A. M. Jones, H. Yu, J. S. Ross, P. Klement, N. J. Ghimire, J. Yan, D. G. Mandrus, W. Yao, and X. Xu, Spin-layer locking effects in optical orientation of exciton spin in bilayer WSe<sub>2</sub>, *Nat. Phys.* **10**, 130 (2014).
- [25] N. C. Fernelius, Properties of gallium selenide single crystal, *Prog. Cryst. Growth Charact. Mater.* **28**, 275 (1994).
- [26] G. B. Abdullaev, L. A. Kulevskii, A. M. Prokhorov, A. D. Savel'Ev, E. Y. Salaev, and V. V. Smirnov, GaSe, a new effective material for nonlinear optics, *JETP Lett.* **16**, 90 (1972).
- [27] K. R. Allakhverdiev, M. O. Yetis, S. Ozbek, T. K. Baykara, and E. Y. Salaev, Effective nonlinear GaSe crystal. Optical properties and applications, *Laser Phys.* **19**, 1092 (2009).
- [28] R. E. Nahory, K. L. Shaklee, R. F. Leheny, and J. C. DeWinter, Stimulated emission and the type of bandgap in GaSe, *Solid State Commun.* **9**, 1107 (1971).
- [29] T. Ugumori, K. Masuda, and S. Namba, Spontaneous and stimulated emission in GaSe under intense excitation, *Solid State Commun.* **12**, 389 (1973).
- [30] J. P. Voitchovsky and A. Mercier, Photoluminescence of GaSe, *Nuovo Cimento Soc. Ital. Fis.* **22B**, 273 (1974).
- [31] A. Mercier and J. P. Voitchovsky, Exciton-exciton and exciton-carrier scattering in GaSe, *Phys. Rev. B* **11**, 2243 (1975).

- [32] T. Moriya and T. Kushida, Luminescence spectra due to exciton-exciton collisions in semiconductors.: I. Spontaneous emission spectra, *J. Phys. Soc. Jpn.* **40**, 1668 (1976).
- [33] T. Moriya and T. Kushida, Luminescence spectra due to exciton-exciton collisions in semiconductors. II. Stimulated emission spectra, *J. Phys. Soc. Jpn.* **40**, 1676 (1976).
- [34] G. Bernier, S. Jandl, and R. Provencher, Spontaneous and stimulated photoluminescence of GaSe in the energy range 2.075–2.125 eV, *J. Lumin.* **35**, 289 (1986).
- [35] L. Pavesi, J. L. Staehli, and V. Capozzi, Mott transition of the excitons in GaSe, *Phys. Rev. B* **39**, 10982 (1989).
- [36] V. Capozzi, L. Pavesi, and J. L. Staehli, Exciton-carrier scattering in gallium selenide, *Phys. Rev. B* **47**, 6340 (1993).
- [37] K. C. Mandal, A. Mertiri, G. W. Pabst, R. G. Roy, Y. Cui, P. Battacharya, M. Groza, A. Burger, A. M. Conway, R. J. Nikolic, A. J. Nelson, and S. A. Payne, Layered III-VI chalcogenide semiconductor crystals for radiation detectors, *Proc. SPIE Int. Soc. Opt. Eng.* **7079**, 70790O (2008).
- [38] D. Marcuse, in *Theory of Dielectric Optical Waveguides*, 2nd Ed. (Academic Press, San Diego, 1991), pp. 1–59.
- [39] H. R. Gutiérrez, N. Perea-López, A. L. Elías, A. Berkdemir, B. Wang, Lv. Ruitao, F. López-Urías, V. H. Crespi, H. Terrones, and M. Terrones, Extraordinary room-temperature photoluminescence in triangular WS<sub>2</sub> monolayers, *Nano Lett.* **13**, 3447 (2013).
- [40] Y. Tang, W. Xie, K. C. Mandal, J. A. McGuire, and C. W. Lai, Exciton spin dynamics in GaSe, *J. Appl. Phys.* **118**, 113103 (2015).
- [41] P. Dey, J. Paul, G. Moody, C. E. Stevens, N. Glikin, Z. D. Kovalyuk, Z. R. Kudrynskiy, A. H. Romero, A. Cantarero, D. J. Hilton, and D. Karaiskaj, Biexciton formation and exciton coherent coupling in layered GaSe, *J. Chem. Phys.* **142**, 212422 (2015).
- [42] C. Weisbuch and B. Vinter, *Quantum Semiconductor Structures: Fundamentals and Applications* (Academic Press, London, 1991).
- [43] R. Sooryakumar, D. S. Chemla, A. Pinczuk, A. C. Gossard, W. Wiegmann, and L. J. Sham, Valence band mixing in GaAs-(AlGa)As heterostructures, *Solid State Commun.* **54**, 859 (1985).
- [44] R. Sooryakumar, A. Pinczuk, A. C. Gossard, D. S. Chemla, and L. J. Sham, Tuning of the Valence-Band Structure of GaAs Quantum Wells by Uniaxial Stress, *Phys. Rev. Lett.* **58**, 1150 (1987).
- [45] J. S. Weiner, D. S. Chemla, D. A. B. Miller, H. A. Haus, A. C. Gossard, W. Wiegmann, and C. A. Burrus, Highly anisotropic optical properties of single quantum well waveguides, *Appl. Phys. Lett.* **47**, 664 (1985).
- [46] K. Ogawa, T. Katsuyama, and H. Nakamura, Polarization Dependence of Excitonic-Polariton Propagation in a GaAs Quantum-Well Waveguide, *Phys. Rev. Lett.* **64**, 796 (1990).
- [47] S. Pfalz, R. Winkler, N. Ubbelohde, D. Hägele, and M. Oestreich, Electron spin orientation under in-plane optical excitation in GaAs quantum wells, *Phys. Rev. B* **86**, 165301 (2012).
- [48] S. Wu, S. Buckley, J. R. Schaibley, L. Feng, J. Yan, D. G. Mandrus, F. Hatami, W. Yao, J. Vučković, A. Majumdar, and X. Xu, Monolayer semiconductor nanocavity lasers with ultralow thresholds, *Nature (London)* **520**, 69 (2015).
- [49] Y. Ye, Z. J. Wong, X. Lu, H. Zhu, X. Chen, Y. Wang, and X. Zhang, Monolayer excitonic laser, [arXiv:1503.06141](https://arxiv.org/abs/1503.06141).
- [50] S. Schwarz, S. Dufferwiel, P. M. Walker, F. Withers, A. A. P. Trichet, M. Sich, F. Li, E. A. Chekhovich, D. N. Borisenko, N. N. Kolesnikov, K. S. Novoselov, M. S. Skolnick, J. M. Smith, D. N. Krizhanovskii, and A. I. Tartakovskii, Two-dimensional metal-chalcogenide films in tunable optical microcavities, *Nano Lett.* **14**, 7003 (2014).
- [51] X. Liu, T. Galfsky, Z. Sun, F. Xia, E.-C. Lin, Y.-H. Lee, S. Kéna-Cohen, and V. M. Menon, Strong light-matter coupling in two-dimensional atomic crystals, *Nat. Photonics* **9**, 30 (2014).
- [52] X. Gan, Y. Gao, K. F. Mak, X. Yao, R.-J. Shiue, A. van der Zande, M. E. Trusheim, F. Hatami, T. F. Heinz, J. Hone, and D. Englund, Controlling the spontaneous emission rate of monolayer MoS<sub>2</sub> in a photonic crystal nanocavity, *Appl. Phys. Lett.* **103**, 181119 (2013).
- [53] S. Wu, S. Buckley, A. M. Jones, J. S. Ross, N. J. Ghimire, J. Yan, D. G. Mandrus, W. Yao, F. Hatami, J. Vučković, A. Majumdar, and X. Xu, Control of two-dimensional excitonic light emission via photonic crystal, *2D Mater.* **1**, 011001 (2014).
- [54] C. Gärtner, C. Karnutsch, U. Lemmer, and C. Pflumm, The influence of annihilation processes on the threshold current density of organic laser diodes, *J. Appl. Phys.* **101**, 023107 (2007).
- [55] B. E. Little and S. T. Chu, Toward very large-scale integrated photonics, *Opt. Photonics News* **11**, 24 (2000).
- [56] R. Nagarajan *et al.*, Large-scale photonic integrated circuits, *IEEE J. Sel. Top. Quantum Electron.* **11**, 50 (2005).
- [57] R. G. Beausoleil, Large scale integrated photonics for twenty-first century information technologies, *Found. Phys.* **44**, 856 (2014).